ACS Chapter Nigeria Book of Proceedings
ISBN: 978-978-68-0485-9 DOI: https://doi.org/10.55455/acsnigeria.1.2.114-126

Eco-friendly Algal-Based Zinc Oxide Nanoparticles for Corrosion Protection of Steel in Acidic Media

Omotola Michael Fayomi[1*], Sonter Camillus Iorumbur[1], James Asamu Akande[2], Idirisu Jibril Limangba[3], and Moses Saviour Iorungwa[1]
[1]Department of Chemistry, Joseph Sarwuan Tarka University, Makurdi.
[2]Department of Chemistry and Biochemistry, Caleb University, Imota Lagos.
[3]Department of Chemistry, Baze University, Abuja.
Corresponding Author's email: omotolafayomi@gmail.com

ABSTRACT

Adding corrosion inhibitor in corrosive medium is one of the effective methods to solve the corrosion of steel materials. Nanomaterials, particularly zinc oxide nanoparticles (ZnO-NPs), have emerged as promising corrosion inhibitor due to their high surface area, reactivity and biocompatibility. The research is based on green synthesis of zinc oxide nanoparticles using *Oedogonium species* aqueous extract, followed by the evaluation of corrosion inhibition on mild steel in 0.5 M HCl aqueous solution. The green synthesized metal oxide nanoparticles were characterized by Scanning Electron Microscopy-Energy-Dispersive X-ray spectroscopy (SEM-EDX), Fourier Transform Infrared Spectroscopy (FT-IR), UV-spectroscopy and powder x-ray diffractometer (PXRD). The formation of zinc oxide nanoparticles was confirmed by the presence of an absorption peak between 410 and 420 nm using UV–visible spectrophotometer. SEM image revealed the average particle size of 15 nm. Elemental component in the nano-particles were determined by EDX and crystallographic structure was monitored by PXRD. Weight loss method was used and revealed a maximum inhibition efficiency of 81% at 0.2g/L, by exposing mild steel samples to corrosive environments in the presence and absence of nanomaterial, the weight loss was calculated over time to determine the effectiveness of the protective layer.

KEYWORDS: Inhibition Efficiency, *Oedogonium sp.*, PXRD, Zinc oxide NPs, weight loss, and Hydrochloric acid

1. INTRODUCTION

Nanotechnology brings together science and engineering to work with materials at incredibly small scales—usually between 1 and 100 nanometers [1]. One area where nanotechnology shows promise is in addressing corrosion, a persistent issue for industries that rely on mild steel. This metal is popular in construction, automotive, and chemical processing due to its strength and low cost, but it doesn't hold up well in acidic environments—such as those found in cleaning processes, pickling, or oil well acid treatments [2].Recent advancements in nanotechnology have opened new avenues for corrosion protection, particularly through the development of high-performance coatings, self-healing materials, and nanoalloys. For example, nanocoatings have proven effective in shielding steel pipelines from harsh, corrosive environments by enhancing surface durability [3]. Zinc oxide nanoparticles (ZnO NPs) have gained considerable attention as effective corrosion inhibitors, largely due to their high surface area, chemical reactivity, and biocompatibility [4]. Among metal oxide nanoparticles (MO-NPs), ZnO stands out for its multifunctional protective mechanisms. One of the primary modes of protection involves the formation of a compact, adherent layer on the metal surface, serving as a physical barrier that limits exposure to corrosive agents like moisture, oxygen, and chloride ions [5]. Their electrocatalytic properties can further inhibit cathodic reactions by restricting oxygen diffusion, while hydrophobic coatings derived from these materials help reduce water ingress—an essential factor in corrosion prevention [6]. Due to these multifunctional attributes, ZnO NPs coatings are widely utilized in industries where corrosion resistance is critical. The nanoparticles' ability to form dense, uniform layers enhances both the durability and protective capability of coatings, while their photocatalytic behaviour supports broader applications in self-cleaning materials, pollution control, and solar energy systems [7]. Despite their effectiveness, conventional methods for synthesizing nanoparticles—such as laser ablation [8] and thermal decomposition [9] —are often costly, energy-intensive, and carry environmental and safety concerns. As a result, there has been a growing shift toward more sustainable and affordable synthesis techniques over the past decade. Among these, biosynthesis has emerged as a particularly promising alternative. This method relies on naturally derived biological materials, including plant extracts [10], algae [11], fungi [12], and yeast [13], to reduce metal salts and facilitate nanoparticle formation.

Green algae have gained attention as an effective and sustainable source for synthesizing zinc oxide nanoparticles (ZnO NPs), owing to their abundance of bioactive compounds such as phenols, flavonoids, and proteins. These natural components play a key role in reducing and stabilizing metal precursors during nanoparticle formation. Unlike traditional synthesis methods—such as sol-gel [14] and chemical vapour deposition [15] —which tend to be costly, resource-heavy, and environmentally harmful the green synthesis route offers a cleaner, more energy-efficient alternative. Recent studies have shown that ZnO NPs synthesized from algae species like *Sargassum muticum* possess strong corrosioninhibiting properties, particularly in acidic conditions. Their nanoscale size and high surface area enable better interaction with corrosive agents enhancing their ability to protect metal surfaces [16].

Meanwhile, the earlier studies demonstrated that green algae extracts alone can effectively inhibit corrosion in acidic media—achieving up to 93% protection on austenitic steel with only 100 ppm [17] and 91% on mild steel at 1M HCl concentrations [18] —there had been little investigation into combining these natural inhibitors with the superior physicochemical properties of nanoparticles. Emerging studies have now confirmed that ZnO nanoparticles synthesized using green algae like *Ulva fasciata* and *Cladophora glomerata* not only retain the eco-friendly characteristics of the plant extract but also significantly enhance the corrosion inhibition of mild steel in acidic environments [19,20]. These biogenically synthesized nanoparticles exhibit high surface area, reactivity, and uniformity—traits that allow them to adsorb effectively onto metal surfaces and form protective barriers. Their integration with algal compounds enhances their stability and performance, offering a dual benefit of sustainability and efficiency in corrosion prevention. This study aims to evaluate the corrosion inhibition performance of zinc oxide nanoparticles (ZnO-NPs) synthesized using the green alga *Oedogonium species* as a natural capping and stabilizing agent. The ZnO-NPs were characterized using standard analytical techniques, and their effectiveness in preventing mild steel corrosion in 0.5 M HCl was assessed through the weight loss method. The goal is to develop a sustainable, eco-friendly alternative to traditional corrosion inhibitors.

2. MATERIALS AND METHODS

2.1. Materials

Zinc nitrate hexahydrate ($Zn(NO_3)_2 \cdot 6H_2O$), sodium hydroxide (NaOH), ethanol 99.9% of analytical grade (Molychem products) were obtained from a commercial dealer and used without any additional reagents. All the glassware was washed with deionized water and oven dried. The green algae, *Oedogonium sp.* were freshly collected from River Benue, Makurdi Nigeria, and were identified in the Department of Botany of Joseph Sarwuan University, Makurdi, Nigeria. The deionized water was used for all the homogenization process.

2.2 Preparation of crude extract

The Green Algae, *Oedogonium sp.*, after collection were severally washed to remove dirt, air-dried for days, pulverized, sieved and stored in an airtight container. For extract preparation 24 g fine powder of *Oedogonium sp.*, was added into 400 mL deionized water. Then it was heated at 60°C for 1 hour. The obtain extract was filtered using filter paper (Whatman no. 1) and stored at 4°C for further use [21].

2.3. Synthesis of ZnO Nanoparticles

The solution of ($Zn(NO_3)_2 \cdot 6H_2O$) was prepared in deionized water. For the preparation of zinc oxide NPs, the flask containing zinc nitrate (11.9g, 0.2M) in 320 mL was reacted with 80 mL of the aqueous *Oedogonium sp.* (algae) Extract the addition of 2M NaOH and stirred using a magnetic stirrer heated at 70°C and stirring was nonstop until a homogenous mixture of the solution was attained. The colour changes from brown solution to pale green paste solution. The product was centrifuged and dried in the oven at 75°C for 48 hours. The particles with brown color obtained were calcined at 500°C for 2 hours in a muffle furnace to give white zinc oxide nanoparticles [22].

2.4 Characterization of Algal-mediated ZnO NPs

The biosynthesized zinc oxide (ZnO) nanoparticles were characterized using UV–Vis, FTIR, XRD, and SEM techniques. UV–Vis spectra were recorded on a JENWAY 6405 spectrophotometer within 200–600 nm to confirm nanoparticle formation. FTIR analysis using an Agilent 630 Cary spectrometer identified functional groups involved in nanoparticle reduction and stabilization, with spectra obtained from KBr pellets (4% w/w) in the 400–4000 cm^{-1} range.

XRD patterns were collected using a Rigaku Miniflex 600 diffractometer (Cu Kα, λ = 1.5406 Å, 40 kV, 30 mA) to determine crystallinity, lattice parameters, and grain size. Surface morphology and particle distribution were examined with a Phenom ProX SEM, revealing particle structure, porosity, and aggregation behavior of the ZnO nanoparticles.

2.5 Weight Loss Measurement

The corrosion inhibition performance of ZnO nanoparticles on mild steel in 0.5 M HCl solution was evaluated using a gravimetric method, adapted from standard procedures commonly used in corrosion studies [23]. Mild steel coupons were initially cleaned, dried and weighed before being immersed in hydrochloric acid solutions with and without varying concentrations of ZnO nanoparticles at 303 K for a duration of 3 hours. After immersion, the samples were rinsed thoroughly with distilled water and acetone, dried and reweighed to determine the mass loss. All experiments were conducted in triplicate to ensure accuracy and the average values were used to calculate the corrosion rate (C_R), inhibition efficiency (IE %) and surface coverage (θ) were calculated using equations (1), (2), and (3) respectively

$$\text{Corrosion rate } (g/h/cm^2) = \frac{\Delta w}{At} \quad (1)$$

where Δw is the weight loss in milligrams of the coupons before and after in immersion(g), *A* is the surface area of the metal coupon in (cm^2), t is the period of immersion in hours.

$$\text{Inhibition efficiency (IE \%)} = \left(\frac{W_0 - W_1}{W_0}\right) \times 100 \quad (2)$$

$$\text{Surface Coverage } (\theta) = \left(\frac{W_0 - W_1}{W_0}\right) \quad (3)$$

where W_0 and W_1 represent the weight losses of the steel in the absence and presence of the ZnO nanoparticles, respectively.

The procedure was repeated at temperature values of 303, 313, 323 and 333K.

2.6 Determination of Activation Energy (E_a)

The plot of log C_R against I/T in equation 4 give a slope (5) from which the activation energy E_a was estimated. The Arrhenius equation described the relationship between the corrosion rate (C_R) and temperature (T) [24].

$$\log CR = \frac{-E^a}{2.303RT} + \log y \quad (4)$$

$$\text{Slope} = \frac{-E^a}{2.303R} \quad (5)$$

E_a is the activation energy, R is the gas constant, T is the temperature in Kelvin and y is the exponential factor.

2.7 Determination of Enthalpy and Entropy Change

The enthalpy change (ΔH) and entropy change (ΔS) were calculated using the transition state theory. An alternative of the transition theory is the Arrhenius Equation.

$$C_R = \frac{RT}{N_h} \exp\left(\frac{\Delta S}{R}\right) \exp\left(\frac{-\Delta H}{R}\right) \quad (6)$$

The linear form of the above equation is

$$Log\left(\frac{CR}{T}\right) = log\left(\frac{R}{Nh}\right) + log\{exp(\frac{\Delta S}{R})\} + log[exp(-\frac{\Delta H}{RT})] \quad (7)$$

Since $Log\, e^x = \frac{x}{ln10}$, equation 7 becomes

$$Log\left(\frac{\overline{CR}}{T}\right) = log\left(\frac{\overline{R}}{Nh}\right) + \left(\frac{\overline{\Delta S}}{ln10}\right) + \left(\frac{\overline{-\Delta H}}{2.303R}\right) \quad (8)$$

$$Log\, C_{RT} = \frac{-\Delta H}{2.303R}(1/T) + log\, {}^{R}_{N}h + (2.^{\Delta}_{303}S) \quad (9)$$

Where h, is the plank constant, N is the Avogadro's number ΔS is the entropy change and ΔH is the enthalpy change. The change in enthalpy ΔH and entropy change ΔS were evaluated from the plot of $\overline{Log\, C_{RT}}$ against $1/T$.

2.7.1 Adsorption isotherm and adsorption constant

The nature of corrosion inhibition has been deduced in terms of the adsorption characteristics of the inhibitor on how the nanoparticles adsorb on the metal surface. The adsorption isotherm model that best describes the adsorption of Zinc oxide nanoparticles on mild steel in 0.5 M HCl solution was obtained by fitting the concentration and the degree of surface coverage of the inhibitor θ into the various adsorption isotherm models. These isotherms include Langmuir, Freundlich and Tempkin were expressed in their linear form as:

The Langmuir adsorption isotherm model;

$$\frac{C}{\theta} = \frac{1}{K_{ads}} + C \quad (10)$$

Freundlich adsorption isotherm model:

$$\log \theta = \log (K_f) + n\log C \quad (11)$$

Tempkin adsorption isotherm model;

$$\theta = lnC + K_{ads} \quad (12)$$

2.7.2 Determination of adsorption thermodynamics parameters

The expression for Gibb's free energy change of adsorption ΔG_{ads} presented in Equation 9 was used to investigate the feasibility and the nature of the adsorption.

$$\Delta G_{ads} = -RTln(55.5K_{ads}) \quad (13)$$

K_{ads} is the adsorption equilibrium constant obtained from the isotherm and the number 55.5 is the molar concentration of water in solution.

3. RESULTS AND DISCUSSION

3.1 UV/Visible Analysis of ZnO nanoparticles

The UV–Vis spectrum (Figure 1) confirmed the successful biosynthesis of ZnO nanoparticles using *Oedogonium sp.* extract. The extract exhibited a strong band near 232 nm, associated with phytochemicals acting as reducing and stabilizing agents. After synthesis, a distinct peak at ~300 nm appeared, characteristic of ZnO nanoparticles and their excitonic transitions [25]. The absence of this ZnO-specific peak in the pure extract and its appearance in the product clearly demonstrate the role of algal biomolecules in nanoparticle formation.

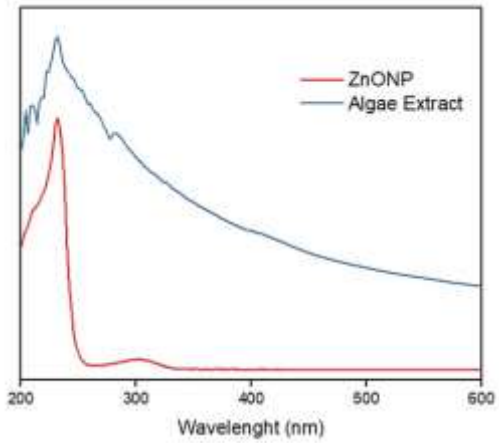

Figure 1: UV-Visible Analysis of ZnO Nanoparticles and the Algae Extract

3.2 Fourier Transform Infra-red (FT-IR) analysis of ZnO nanoparticle:

FTIR analysis was performed to identify the functional groups involved in ZnO nanoparticle formation [26]. As shown in Figure 2, the broad absorption band around 3420–3510 cm^{-1} corresponds to O–H stretching vibrations from surface-adsorbed water or hydroxyl groups, indicating hydrogen bonding with phytochemicals used during green synthesis [27]. Peaks observed below 1000 cm^{-1} are characteristic of Zn–O bond vibrations within the nanoparticle matrix [28]. These features confirm the presence of phytochemical functional groups and the successful formation of Zn–O linkages, which enhance the nanoparticles' surface reactivity and catalytic potential.

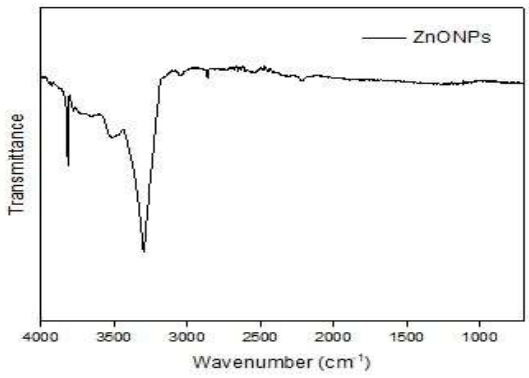

Figure 2: Fourier transform infrared spectrometer (FTIR) Analysis of ZnO Nanoparticles

3.3 *Scanning Electron Microscopy (SEM) Analysis* of *ZnO Nanoparticles*

Scanning Electron Microscopy (SEM) was used to examine the morphology of the synthesized ZnO nanoparticles (Figure 3). The images revealed rod-shaped structures with well-defined pores, confirming effective nanoparticle formation on the nanocomposite surface. These open pores suggest strong electrostatic interactions between the *Oedogonium sp.* extract and ZnO, supporting their potential effectiveness in corrosion inhibition.

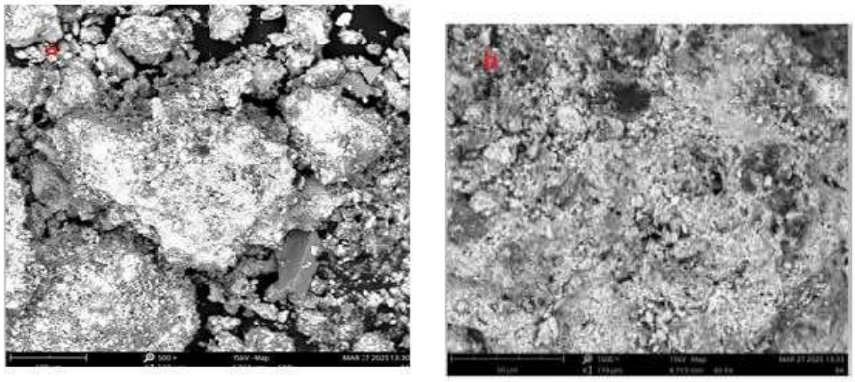

Figure 3: SEM images of Zinc Oxide Nanoparticles derived from *Oedogonium sp.* Extract (a) 5 µm (b) 1 µm

3.4 *Energy Dispersive X-Ray Spectroscopy (EDX) analysis*

The EDX spectrum (Figure 4) confirmed the formation of pure ZnO nanoparticles, showing dominant Zn Kα/Kβ and O Kα peaks with near-stoichiometric ratios. The absence of major impurity peaks indicates high purity, while a minor carbon signal likely originates from residual biomolecules or carbon tape [29]. Atomic composition revealed Zn (58.24–85.03 wt.%), with small amounts of C (7.07%) and N (3.14%) from algal metabolites acting as capping agents. These results verify the successful green synthesis of ZnO nanoparticles with high compositional purity, supporting their suitability for corrosion inhibition and other applications such as photocatalysis and biomedicine [30,31].

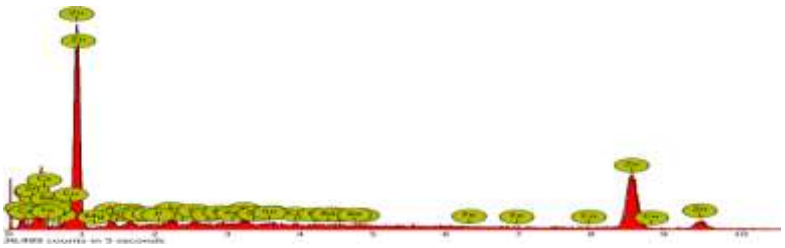

Figure 4: EDX of the Zinc Oxide Nanoparticles

3.5 *X-ray diffraction (XRD) Analysis of ZnO Nanoparticle*

Figure 5 displays the X-ray diffraction (XRD) spectrum of ZnO nanoparticles. It possesses a high level of crystallinity, illustrated by sharp and intense diffraction peaks. The diffractogram presents major peaks at 2 theta angles of the crystal planes (100), (002), (101), (102), (110), (103), (112), and (201) that correspond to the JCPDS card no. 04-008-8199 and can be used to specify the hexagonal wurtzite structure of ZnO [32]. These peaks are very clear, the highest peak occurring at $2\theta = 36.25^0$ is due to the (101) plane, a typical characteristic of a pure and crystalline nanoparticle of Zn-O [33]. No additional peaks are present, which proves that no secondary phases or impurities present; this indicate phase-pure ZnO nanocrystals had been created successfully [34].

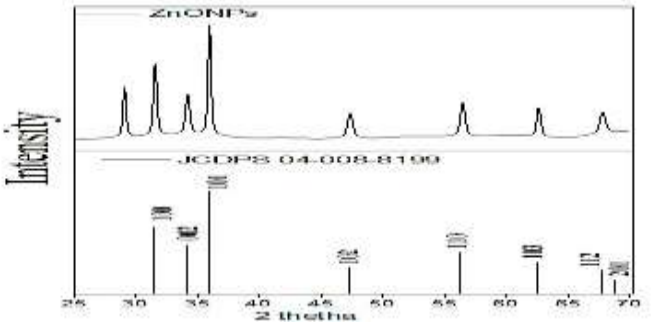

Figure 5: X-ray Diffraction (XRD) pattern of ZnO nanoparticles.

Table 1: Weight Loss (g) of Mild Steel at various concentrations of Algal-mediated Zinc oxide Nanoparticles at different Time Intervals

ZnO NPs conc. (g/L)	**Weight Loss (g)**			
	6 h	24 h	48 h	72 h
Blank	0.137	0.140	0.145	0.148
0.05	0.094	0.084	0.098	0.087
0.10	0.072	0.064	0.076	0.060
0.15	0.058	0.049	0.054	0.042
0.20	0.034	0.023	0.032	0.028

Table 2: Inhibition efficiency of various concentration of Algal-mediated Zinc oxide Nanoparticles at different Time Intervals

ZnO NPs conc. (g/L)	Inhibition Efficiency (%)			
	6 h	24 h	48 h	72 h
0.05	31	40	32	41
0.10	48	54	50	60
0.15	58	65	63	72
0.20	75	80	78	81

The experimental findings (Tables 1–8) confirm that algal-mediated ZnO nanoparticles act as efficient corrosion inhibitors through composition-, time-, and adsorption-dependent mechanisms. Weight loss analysis revealed a clear dose-dependent protection, where increased ZnO concentration reduced mass loss (e.g., 0.15 g/L: 0.042 g vs. 0.20 g/L: 0.028 g after 72 h). Optimal inhibition efficiency, reaching up to 92% in acidic media, was achieved at 0.1 wt% ZnO [35]. The nanoparticles form a protective, chemisorbed layer on the steel surface, blocking active corrosion sites and enhancing adhesion through algal biomolecules. This eco-friendly approach demonstrates superior, sustainable corrosion resistance compared to conventional synthetic inhibitors.

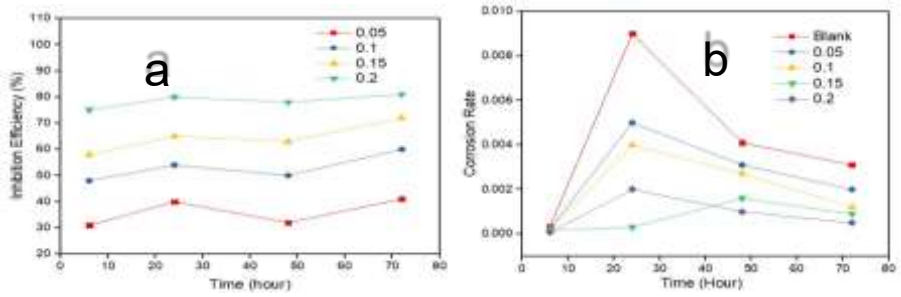

Figure 6: Effect of ZnO-NPs concentrations in 0.5 M HCl at 6 to 72 hours on the (a).inhibitory efficiency (b) corrosion rate

Table 3: Corrosion Rates of Mild Steel at different Time Immersions of Various Algal-mediated Zinc oxide Nanoparticles Concentrations

ZnO NPs conc. (g/L)	Corrosion rate (g/h/cm^2)			
	6 h	24 h	48 h	72 h
Blank	$3.3x10^{-4}$	$9.0x10^{-3}$	$4.1x10^{-3}$	$3.1 x10^{-3}$
0.05	$2.3 x10^{-4}$	$5.0x10^{-3}$	$3.1x10^{-3}$	$2.0 x10^{-3}$
0.10	$1.8 x10^{-4}$	$4.0x10^{-3}$	$2.7x10^{-3}$	$1.2x10^{-3}$
0.15	$1.6 x10^{-4}$	$3.0x10^{-3}$	$1.6x10^{-3}$	$9.0x10^{-4}$
0.20	$8.0 x10^{-5}$	$2.0x10^{-3}$	$1.0x10^{-3}$	$5.0x10^{-4}$

Table 4: Weight Loss (g) of Mild Steel at various concentrations of Algal-mediated Zinc oxide Nanoparticles at different temperatures

ZnO NPs conc. (g/L)	Weight Loss (g)			
	303 K	313 K	323 K	333 K
Blank	0.138	0.136	0.139	0.141
0.05	0.098	0.098	0.097	0.099
0.10	0.073	0.073	0.059	0.077
0.15	0.059	0.054	0.048	0.056
0.20	0.037	0.037	0.027	0.029

Table 5: Inhibition efficiency of Mild Steel at various concentrations of Algal-mediated Zinc oxide Nanoparticles at different temperatures

ZnO NPs conc. (g/L)	Inhibition efficiency (%)			
	303 K	313 K	323 K	333 K
0.05	29	28	30	30
0.10	47	46	50	45
0.15	57	60	66	60
0.20	73	73	81	80

Algal capping agents such as polysaccharides and proteins promote uniform adsorption of ZnO nanoparticles on steel, forming a protective barrier that blocks active sites and restricts acid diffusion. The concentration-dependent behavior follows the Langmuir isotherm, indicating monolayer adsorption where surface coverage increases with nanoparticle concentration. ZnO NPs inhibit both anodic and cathodic reactions, while at higher temperatures, chemisorption dominates through stable Zn^{2+}–alginate complexes bound to steel heteroatoms (O, N). The rise in inhibition efficiency (IE%) with temperature suggests covalent bonding between algal-functionalized ZnO NPs and steel, consistent with the ElAwady kinetic-thermodynamic model of enhanced inhibitor–metal interactions.

Table 6: Corrosion rates of Mild Steel at various concentration of Algal-mediated Zinc oxide Nanoparticles at different temperature

ZnO NPs conc. (g/L)	Corrosion rate (g/h/cm^2)			
	303 K	313 K	323 K	333 K
Blank	$1.06x10^{-3}$	$1.05x10^{-3}$	$1.07x10^{-3}$	$1.08x10^{-3}$
0.05	$8.3 x10^{-4}$	$8.3 x10^{-4}$	$8.2x10^{-4}$	$6.64x10^{-4}$
0.10	$5.3 x10^{-4}$	$5.3x10^{-4}$	$5.0x10^{-4}$	$5.6x10^{-4}$
0.15	$4.4 x10^{-4}$	$4.0x10^{-4}$	$3.6x10^{-4}$	$4.2x10^{-4}$
0.20	$2.5 x10^{-4}$	$2.5x10^{-4}$	$1.9x10^{-4}$	$2.0x10^{-4}$

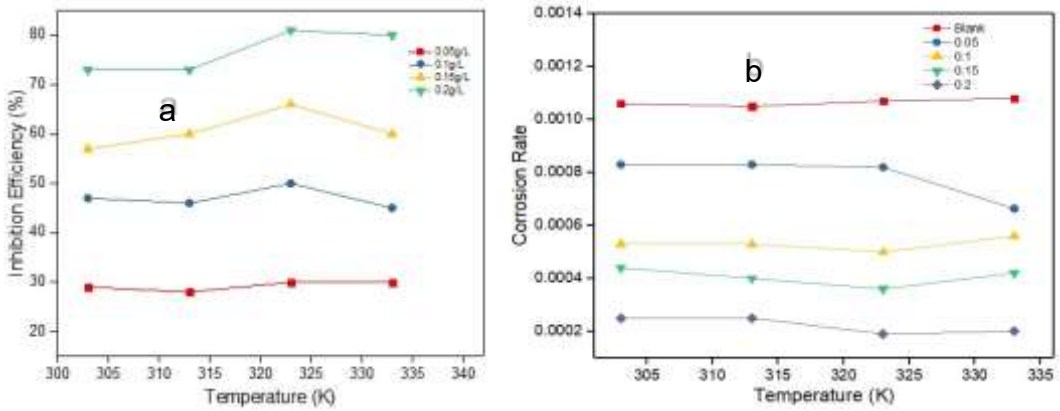

Figure 7: Effect of ZnONPs concentrations in 0.5 M HCl at 303 to 333 K on the (a) inhibitory efficiency (b) corrosion rate

Table 7: Thermodynamic Parameters for the Adsorption of ZnO Nanoparticles on Mild Steel in 0.5 M HCl

ZnONPs (g/L)	E_a (KJ/mol)	ΔH (KJ/mol)	ΔS (J/mol/K)
Blank	0.618	-2.021	-289.543
0.05	5.604	- 8.244	-311.696
0.10	0.824	-1.801	-294.655
0.15	-2.183	-4.823	-311.696
0.20	-7.935	-10.578	-329.503

Table 8: Surface Coverage (θ) of ZnO Nanoparticles on Mild Steel at Various Temperatures

ZnO NPs conc.	Surface Coverage (θ)			
(g/L)	303 K	313 K	323 K	333 K
0.05	0.29	0.28	0.30	0.30
0.10	0.47	0.46	0.50	0.45
0.15	0.57	0.60	0.66	0.60
0.20	0.73	0.73	0.81	0.80

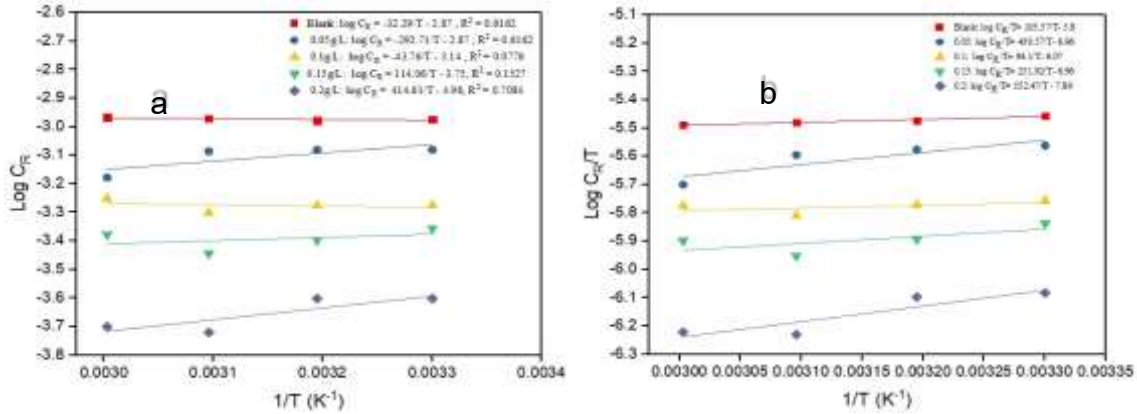

Figure 8: Plots for Determination of Enthalpy and Entropy Change

The thermodynamic results (Table 7) indicate that the adsorption of algal-mediated ZnO nanoparticles on mild steel in 0.5 M HCl is spontaneous and exothermic, as shown by negative activation energy (E_a) and enthalpy change (ΔH). Corrosion rates consistently decreased with increasing ZnO nanoparticle concentration due to thermally stable Zn–alginate complexes that blocked active corrosion sites. A slight rise in corrosion at 333 K suggests minor desorption caused by thermal motion [36]. The transition from positive (+0.62 kJ/mol) to negative Ea values indicates a shift from physical to chemisorption through covalent bonding between algal phenolic groups and iron atoms (Sophie and Antony, 2019). Surface coverage analysis ($R^2 > 0.98$) confirmed monolayer adsorption following the Langmuir model, with the strongest adsorption at 323 K and negative ΔG_ads values confirming spontaneity. Langmuir isotherm best described the adsorption process, while Freundlich and Temkin showed secondary fits. The high K_ads (6.5–7.0 M^{-1}) across temperatures further supports strong, stable binding between ZnO NPs and the steel surface [4].

Table 9: Langmuir Isotherm data

Temperature (K)	Intercept	Slope	R_2	K_{ads} (M^{-1})	ΔG_{ads} (kJ/mol)
303K	0.142	0.710	0.989	7.042	-15.035
313K	0.150	0.637	0.989	6.667	-15.388
323K	0.143	0.537	0.987	6.993	-16.008
333K	0.153	0.556	0.933	6.535	-16.317

Table 10: Freundlich Isotherm data

Temperature (K)	Intercept	Slope	R_2	K_f (M^{-1})	ΔG_{ads} (kJ/mol)
303K	0.566	0.426	0.438	1.766	-11.551
313K	0.569	0.429	0.428	1.757	-11.919
323K	0.713	0.148	0.853	1.402	-11.694
333K	0.688	0.146	0.829	1.453	-12.154

Table 11: Tempkin Isotherm data

Temperature	Intercept	Slope	R_2	K	ΔG_{ads} (kJ/mol)
303K	1.179	0.302	0.969	49.599	-0.019
313K	1.219	0.318	0.935	46.216	-0.018

323K	1.361	0.362	0.882	42.934	-0.019
333K	1.293	0.343	0.832	43.366	-0.019

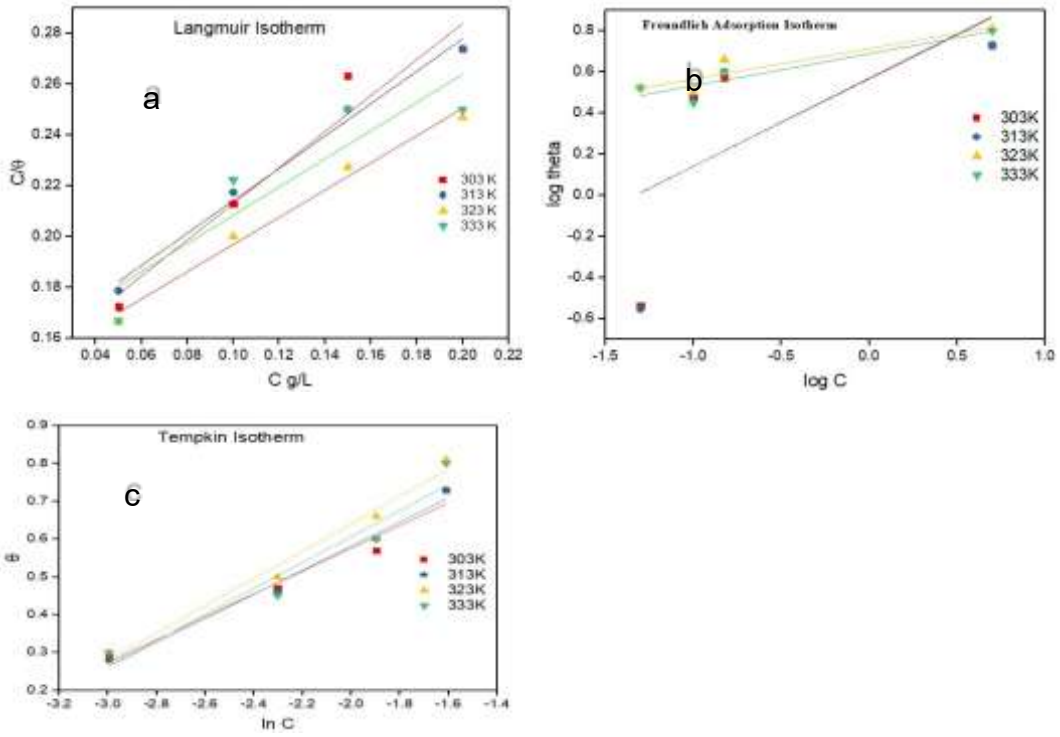

Figure 9: Adsorption isotherms of Algal-mediated ZnO-NPs on the surface of mild steel: (a) Langmuir (b) Freundlich (c) Tempkin

4. CONCLUSION

This study confirms that zinc oxide nanoparticles (ZnO-NPs) can be sustainably synthesized from zinc nitrate hexahydrate using *Oedogonium sp.* extract as a natural reducing and stabilizing agent. Characterization by UV–Vis, FTIR, SEM-EDX, and XRD verified successful nanoparticle formation. Corrosion studies showed that algal-mediated ZnO-NPs effectively protected mild steel in 0.5 M HCl, with inhibition efficiency rising from 73% at 303 K to nearly 80% at 333 K. Adsorption increased with immersion time and followed the Langmuir isotherm, indicating monolayer coverage. Thermodynamic parameters (ΔG°ads, ΔH°ads, ΔS°ads) revealed a spontaneous, exothermic process driven by both chemisorption—via heteroatoms with lone electron pairs—and physisorption through electrostatic attraction. These results highlight green-synthesized ZnO-NPs as promising, eco-friendly corrosion.

CONFLICT OF INTERESTS

The authors declare no conflict of interests.

REFERENCES

(1) Khan, I.; Saeed, K.; Khan, I. Nanoparticles: Properties, applications and toxicities. *Arab. J. Chem.* **2019**, 12, 908–931.

(2) Verma, C.; Olasunkanmi, L. O.; Quadri, T. W.; Sherif, E. S. M.; Ebenso, E. E. Gravimetric, Electrochemical, Surface Morphology, DFT, and Monte Carlo Simulation Studies on Three NSubstituted 2-Aminopyridine Derivatives as Corrosion Inhibitors of Mild Steel in Acidic Medium. *J. Phys. Chem. C* **2018,** 122, 11870–11882.

(3) Shwetha, K.; Praveen, B. M.; Devendra, B. K. A review on corrosion inhibitors: Types, mechanisms, electrochemical analysis, corrosion rate and efficiency of corrosion inhibitors on mild steel in an acidic environment. *Results in Surfaces and Interfaces* **2024**, 16, 100258.

(4) Elebo, A.; Sani, U.; Ekwumemgbo, P. A.; Ajibola, V. O. Green Synthesis and Zinc-Oxide Nanoparticles for Corrosion Inhibition and Modeling Corrosion Inhibition of Mild Steel in HCl Solutions. *Biosens. Nanotheranostics* **2024,** 3, 1-17.

(5) Azmi, H. N. S.; Alam, M. Exploring the Anti-Corrosion, Photocatalytic, and Adsorptive Functionalities of Biogenically Synthesized Zinc Oxide Nanoparticles. *Inorganics* **2024**, 12, 199.

(6) Sampath, S.; Madhavan, Y.; Muralidharan, M.; Sunderam, V.; Lawrance, A.V.; Muthupandian, S. A review on algal mediated synthesis of metal and metal oxide nanoparticles and their emerging biomedical potential. *J. Biotechnol.* **2022**, 360, 92–109.

(7) Gao, H., Li, Q., Dai, Y., Luo, F.; Zhang, H. X. High efficiency corrosion inhibitor 8hydroxyquinoline and its synergistic effect with sodium dodecylbenzenesulphonate on AZ91D magnesium alloy. *Corros. Sci.* **2010**, 52, 1603–1609.

(8) Amendola, V.; Amans, D.; Ishikawa, Y.; Koshizaki, N.; Scirè, S.; Compagnini, G.; Reichenberger, S.; Barcikowski, S.Room-Temperature Laser Synthesis in Liquid of Oxide, Metal-Oxide Core-Shells, and Doped Oxide Nanoparticles. *Chem. - A Eur. J.* **2020,** 26, 9206–9242.

(9) Patil, S. S.; Kamble, V. S.; Patil, D. K.; Pawara, J. M. Synthesis of Metal Oxide Nanoparticles by Thermal Decomposition of a Ni(II) Complex and its Antimicrobial Activity. *Malaysian J. Chem.* **2022,** 24, 125–131.

(10) Fayomi, O. M., Olajide, O. O.; Emmanuel, S. A. Anti-Plasmodial Activity of Iron Oxide Nanoparticles Derived from Moringa Oleifera Stem Bark and Root Extracts. *FUAM J. Pure Appl. Sci.* **2025,** 5, 10–22.

(11) Bhuyar, P.; Rahim, Mohd H. A.; Sundararaju, S.; Ramaraj, R.; Maniam, G. P.; Govindan, N. Synthesis of silver nanoparticles using marine macroalgae *Padina sp*. and its antibacterial activity towards pathogenic bacteria. *Beni-Suef Univ. J. Basic Appl. Sci.* **2020,** 9, 1-15.

(12) Saitoh, N.; Fujimori, R.; Yoshimura, T.; Tanaka, H.; Kondoh, A.; Nomura, T.; Konishi, Y. Microbial recovery of palladium by baker's yeast through bioreductive deposition and biosorption. *Hydrometallurgy* **2020,** 196, 105413.

(13) Das, M.; Saxena, N.; Dwivedi, P. Emerging trends of nanoparticles application in food technology: Safety paradigms. *Nanotoxicology* **2009,** 3(1) 10-18.

(14) Itodo, A. U., Itodo, O. M., Iornumbe, E. & Fayomi, O. M. Progress in Chemical and Biochemical Research Sorptive chelation of metals by inorganic functionalized organic WOx – EDA nanowires : adsorbent characterization and isotherm studies. *Prog. Chem. Biochem. Res.* **2019,** 1, 50–59.

(15) Zhou, X. Q.; Hayat, Zakir; Zhang, Dong-Dong; Li, Meng-Yao; Hu, Si; Wu, Qiong; Cao, Y. F.; Yuan, Y. Zinc Oxide Nanoparticles: Synthesis, Characterization, Modification, and Applications in Food and Agriculture. *Processes* **2023,** 11, 1193.

(16) Sadek, R.F.; Farrag, H. A.; Abdelsalam, S. M; Keiralla, Z. M.H.; Raafat, A. I.; Araby, E. A powerful nanocomposite polymer prepared from metal oxide nanoparticles synthesized Via brown algae as anti-corrosion and anti-biofilm. *Front. Mater.* **2019,** 6, 140.

(17) Verma, D. K.; Khan, F. Green approach to corrosion inhibition of mild steel in hydrochloric acid medium using extract of spirogyra algae. *Green Chem. Lett. Rev.* **2016,** 9, 52–60.

(18) Almanza, E., Del C. G.; Pua, L.; Pineda, Y.; Rozo, W.; Marquez, M.; Fonseca, A. Eco-friendly Chlorella vulgaris extracts for corrosion protection of steel in acidic environments. *Heliyon* **2024,** 10, e39717.

(19) Abdulwahid, K. E.; Dwaish, A. S.; Dakhil, O. A. Green synthesis and characterization of zinc oxide nanoparticles from Cladophora glomerata and its antifungal activity against some fungal isolates. *Plant Arch.* **2019,** 19, 3527–3532.

(20) Balasubramanian, R.; Ravi, S. Green Synthesised Zinc Oxide Nanoparticles from Ulva Fasciata Algae Extract for Antibacterial and Supercapacitor Application. *Int. J. Membr. Sci. Technol.* **2023,** 10, 3089–3099.

(21) Fayomi, O. M.; Olasan, J. O.; Aguoru, C. U.; Anjorin, T. S.; Sule, A. M. Effect of Biosynthesized ZnO Nanoparticles Derived From Jatropha Tajonensis on the Yield of Bambara Groundnut (Vigna Substerranean L.). *African J. Agric. Allied Sci.* **2024,** 4, 192–214.

(22) Fayomi, O. M.; Olasan, J. O.; Aguoru, C. U.; Terhemba, M. S. Growth and Yield Responses of Soybean (Glycine Max L.) to Zinc Oxide (ZnO) Nanoparticles Foliar Application. *Biotechnol. Acta* **2024,** 17, 56–66.

(23) Fayomi, O. M.; Chahul, H. F.; Ike, D. C.; Ndukwe, G. I.; Phoebe, I. M. Thermodynamic and Adsorption Study of the Corrosion Inhibition of Mild Steel by Aframomum chrysanthum Extract in 0.1 M Hydrochloric Acid Solution. *Asian J. Appl. Chem. Res.* **2021,** 8, 64–73.

(24) Mohammedali, D. R.; Salman, H. I.; Bahjat, M. N.; Abood, E. S. Synthesis of new Corrosion Inhibitor from Nano-Polymer and study its adsorption on carbon steel at different Temperatures. *Egypt. J. Chem.* **2022,** 65, 691–705.

(25) Halanayake, K. D.; Kalutharage, N. K.; Hewage, J. W. Microencapsulation of biosynthesized zinc oxide nanoparticles (ZnO-NPs) using Plumeria leaf extract and kinetic studies in the release of ZnO-NPs from microcapsules. *SN Appl. Sci.* **2021,** 3, 1–12.

(26) Pasieczna-Patkowska, S.; Cichy, M.; Flieger, J. Application of Fourier Transform Infrared (FTIR) Spectroscopy in Characterization of Green Synthesized Nanoparticles. *Molecules* **2025,** 30, 684.

(27) Alharbi, F. N., Abaker, Z. M. & Makawi, S. Z. A. Phytochemical Substances — Mediated Synthesis of Zinc Oxide. *Inorganics* **2023,** 11, 328.

(28) Jayachandran, A., Aswathy, T. R. & Achuthsankar, N. S. Green synthesis and characterization of zinc oxide nanoparticles using *Cayratia pedata* leaf extract. *Biochem. Biophys. Reports* **2021,** 26, 100995.

(29) Kaur, H. *et al.* Green synthesis of ZnO nanoparticles using E. cardamomum and zinc nitrate precursor: a dual-functional material for water purification and antibacterial applications. *RSC Adv.* **2025,** 15, 16742–16765.

(30) Chaudhary, R.; Nawaz, K.; Khan, A. K.; Hano, C.; Abbasi, B. H.; Anjum, S. An overview of the algae-mediated biosynthesis of nanoparticles and their biomedical applications. *Biomolecules* **10**, 1–35 (2020).

(31) Mohammadi, A.; Hashemi, N.; Ghassabzadeh, M.; Sharafi, A.; Yazdinezhad, A.; Danafar, H. Green synthesis and toxicological evaluation of zinc oxide nanoparticles utilizing Punica granatum fruit Peel extract: an eco-friendly approach. *Sci. Rep.* **2025,** 15, 20853.

(32) Ramike, M. P.; Ndungu, P. G.; Mamo, M. A. Exploration of the Different Dimensions of Wurtzite ZnO Structure Nanomaterials as Gas Sensors at Room Temperature. *Nanomaterials* **2023,** 13, 2810.

(33) Chand, P.; Gaur, A.; Kumar, A. Structural and optical properties of ZnO nanoparticles synthesized at different pH values. *J. Alloys Compd.* **2012,** 539, 174–178.

(34) Kahouli, M.; Barhoumi, A.; Bouzid, A.; Al-Hajry A.; Guermazi, S. Structural and optical properties of ZnO nanoparticles prepared by direct precipitation method. *Superlattices Microstruct.* **2015,** 85, 7–23.

(35) Alprol, A. E.; Mansour, A. T.; El-Beltagi, H. S.; Ashour, M. Algal Extracts for Green Synthesis of Zinc Oxide Nanoparticles: Promising Approach for Algae Bioremediation. *Materials (Basel).* **2023,** 16, 2819.

(36) Kamburova, K.; Boshkova, N.; Radeva, T.; Boshkov, N. Smart Zinc-Based Coatings with Chitosan–Alginate Nanocontainers Loaded with ZnO and Caffeine for Corrosion Protection of Mild Steel. *Metals (Basel).* **2025,** 15, 65.

(37) Sophie, P. L.; Antony, N. Kinetic, Thermodynamic and Adsorption Isotherm Analysis for the Corrosion Inhibition of Carbon Steel in Aqueous Media by Lippia Nodiflora. *J. Emerg. Technol. Innov. Res.* **2019,** 6, 217–229.